High Permittivity Anisotropic 3D Printed Material

Aaron Harmon
Dept. of Electrical and
Computer Engineering –
Electromagnetic Compatibility
Laboratory
Missouri University of Science
and Technology
Rolla, MO, USA
afhpq4@umsystem.edu

Victor Khilkevich
Dept. of Electrical and
Computer Engineering –
Electromagnetic Compatibility
Laboratory
Missouri University of Science
and Technology
Rolla, MO, USA
khilkevichv@umsystem.edu

Kristen M. Donnell
Dept. of Electrical and
Computer Engineering –
Microwave Sensing (µSense)
Laboratory
Missouri University of Science
and Technology
Rolla, MO, USA
kmdgfd@umsystem.edu

Abstract— In this work, the diagonal elements of the permittivity matrix for dielectric samples, 3D printed with a carbon fiber-loaded material (XT-CF20), are measured for frequencies within the range of 1 MHz to 18 GHz. These permittivity measurements demonstrated a strong anisotropy, indicating that the electromagnetic properties of the CF20 material depend on the infill method used to print. The importance of understanding the anisotropy for microwave device design is demonstrated via a dielectric-loaded cavity resonator application.

Keywords—3D Printing, Anisotropic Materials, Spatial Permittivity Components, Dielectric Materials

I. INTRODUCTION

3D printing is a well-established additive manufacturing technology that successively adds geometric layers of material to create the desired object. This technology is commonly realized via the Fused Deposition Modeling (FDM) method where the added material, referred to as the filament, is first melted, and then deposited to create a thin layer of new material that is fused to previous layers during the fabrication process. Filament types include traditional polylactic acid (PLA) plastic-based filaments as well as more advanced materials that have been infused with different additives such as carbon fiber, graphite, metallic particles, etc. These specialty filaments are designed primarily to have unique mechanical properties when compared to traditional PLA. However, the inclusion of different additives in these specialty filaments also changes their electromagnetic properties.

The technology of 3D printing has recently been incorporated into the field of electromagnetics for prototyping and production of devices such as absorbers, antennas, frequency selective surfaces (FSSs), and sensors. [1-9]. In [1] and [2], electromagnetic absorbers were printed using specialty filaments infused with carbon fiber and graphite, respectively. Moreover [3] extends this idea, demonstrating how one can create specialty filaments doped with nano and advance materials and then use such filaments in EMC applications such as absorbers for EMI shielding.

In [4] and [5], filaments doped with metallic powders were used to construct FSSs. Further, in [6-8], both conductive and dielectric 3D printed antennas are demonstrated. Finally, in [9] examples of nanotechnology-enabled additively manufactured RF and millimeter-wave electronics are given.

Generally speaking, for any 3D printed object intended for high-frequency applications (including those mentioned above), the filament's electrical properties must be known to ensure the intended operation and hence a successful application. In [10], the electrical properties of the colorFabb XT-CF20 [11] carbon fiber loaded filament (CF20) material

were investigated (among many other materials). The reported relative permittivity from this investigation was relatively low (approximately 4.7-4.3, [10] table 4, material No. 7), with no report on signs of anisotropy for the CF20 material.

Contrary to the results reported in [10], this work demonstrates that the permittivity of the CF20 material strongly depends on the orientation of the electric field with respect to the printed layers of the measured sample and for some orientations is much higher than previously reported (around 20 or greater). To this extent, in this paper, the diagonal components of the complex permittivity matrix are measured for 3D printed CF20 dielectric samples. Specifically, Section II reviews the measurement methods used to measure the permittivity of a dielectric sample. Section III reports the results of such measurements for the dielectric samples. Section IV demonstrates the anisotropic effect in the performance of a dielectric cavity up to 20 GHz, highlighting the importance of a proper understanding of the electrical properties of the material. Finally, future work and conclusions are discussed in Section V.

II. PERMITTIVITY EXTRACTION METHODS

In this work, three permittivity extraction methods were employed: the capacitive method [12], the coaxial airline [13 – 14] method, and the open-ended waveguide (OEWG) method employing a modified flange design [15 – 16].

A. Capacitive Method (1 MHz – 300 MHz)

For the capacitive method [12], a slab of the printed dielectric material is sandwiched between two metallic plates, thereby creating a parallel plate capacitor. The capacitance of this capacitor can be calculated from impedance measurements. This capacitance is then used to calculate the complex permittivity of the dielectric material between the two plates.

For frequencies from 1 MHz to 300 MHz, the impedance of the capacitor is calculated from reflection coefficient (S_{11}) measurements made using an Agilent E5071C Vector Network Analyzer (VNA). A one-port SOL calibration and port extension are first performed for port 1 of the VNA to account for the parasitics of the coaxial cable used to connect the capacitor to the VNA. The center and outer conductor of this coaxial cable are then mechanically clamped to the parallel plate capacitor and the complex reflection coefficient of the capacitor is recorded. An image of this measurement is shown in Figure 1.

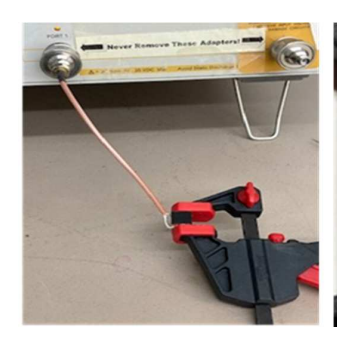




Fig. 1. (Left) An image of the parallel plate capacitor connected to the VNA via a coaxial cable and mechanical clamping. (Right) An image of the mechanical clamping used in this measurement. The red blocks are the jaws of the clamp, the black cube is the printed CF20 sample, and the silver wires are the center conductor and shield of the coaxial cable used to connect the parallel plate capacitor to the VNA for measurement.

The reflection coefficient (S_{11}) to impedance and impedance to capacitance conversion is done using (1) and (2):

$$Z = Z_0 \left[\frac{1 + S_{11}}{1 - S_{11}} \right] = R_c + jX_c \tag{1}$$

$$C = -\frac{1}{\omega X_C} \tag{2}$$

where Z_0 is the port impedance of the VNA, nominally 50 Ω , S_{11} is the measured reflection coefficient of the capacitor, Z is the calculated complex impedance of the capacitor, and X_c is the reactive component of the calculated impedance. The permittivity of the dielectric is then calculated using the parallel plate capacitor formula shown in (3):

$$\varepsilon_r = \frac{CD}{\varepsilon_0 A} \tag{3}$$

where C is the calculated capacitance for the capacitor, D is the distance between the two plates, ε_0 is the permittivity of vacuum, and A is the area of the plates. It is important to note that the fringing fields of the capacitor are neglected in (3). These fringing fields are assumed to be relatively weak when compared to the fields between the plates in the high permittivity material and hence can be neglected.

B. Coaxial Airline Method (700 MHz – 18 GHz)

The coaxial airline method relies upon the air-filled transmission line method implemented in Keysight's 85071 material characterization software [17]. For this method, an air-filled coaxial transmission line (coaxial airline) with an inner diameter of 7 mm is first attached to a Keysight N5225A Precision Network Analyzer (PNA). Next, the PNA was calibrated using a TRL calibration routine. After this, a toroidal dielectric sample is placed inside of the airline and the complex transmission and reflection coefficients of the sample are measured. The software then calculates the permittivity and permeability of the sample.

C. OEWG Method (8.2 GHz – 12.4 GHz)

Open-ended rectangular waveguide probes have been used for microwave dielectric material characterization [15]. This process is done by measuring the complex reflection coefficient of an OEWG probe radiating into a single- or multi-layered structure backed by infinite half-space or a conductor. These measurements are completed using a calibrated VNA. The measured reflection coefficient is then used in conjunction with the forward model to calculate the complex permittivity of the layered structure. As it relates to

measurement, the finite flange of the OEWG contributes to measurement error. As such, a modified flange was introduced in [16] which substantially improved the accuracy of the measurement technique.

III. PERMITTIVITY MEASUREMENT FOR THE CF20 SAMPLES

A. Samples Measured in this Work

All CF20 samples measured in this work were 3D printed on a Jubilee 3D printer [18] using a layer height of 0.2 mm with a 0.4 mm stainless steel nozzle. Each sample was printed with 100% infill, however, the type of infill used varied between samples (as is detailed below).

The cubic CF20 samples measured using the capacitive method were printed with a 45-degree rectilinear infill pattern. This infill pattern was rotated 90 degrees around the Z-axis for each printed layer, making the samples symmetric in the X and Y planes, as illustrated in Figure 2. The cubic samples had a side length of 10 mm. When the X and Y components of the permittivity are measured, the electric field vector is parallel to the layers of the sample. However, when the Z component of the permittivity is measured, the electric field vector is perpendicular to the layers of the sample. Figure 2 shows a rendering of these samples.

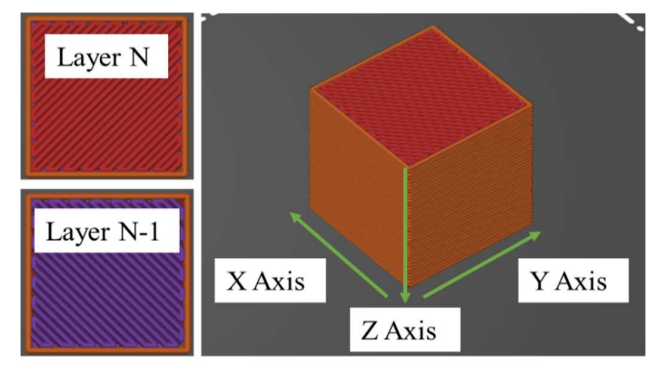


Fig. 2. (Left) Infill pattern used to print the cubic samples. (Right) Orthographic view of the 3D printed cubic sample with axis annotations.

The toroidal samples measured using the airline method were printed with concentric cylindrical infill. The toroidal samples had an inner diameter of 3 mm, an outer diameter of 7 mm, and a height of 3 mm. For these samples, the electric field vector is parallel to the layers of the sample but perpendicular to the vertical walls of the perimeters and the infill. Figure 3 shows a rendering of these samples. The arrows in Figure 3 represent the electric field vector.

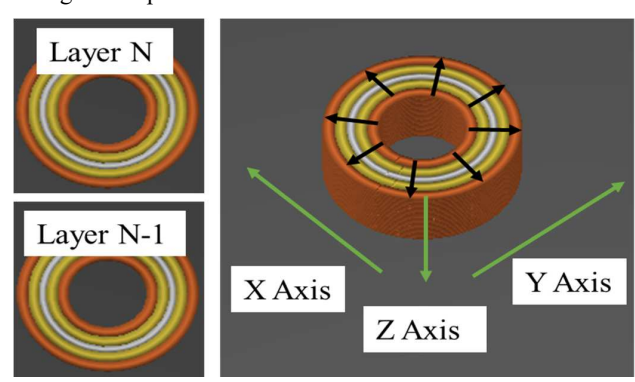


Fig. 3. (Left) Infill pattern used to print the toroidal sample. (Right) Orthographic view of the 3D printed toroidal sample with axes annotations. The arrows shown represent the electric field vector.

The slab samples measured using the OEWG method were printed the same as the cubic samples, using a 45-degree rectilinear infill pattern that was rotated 90 degrees around the Z-axis for each printed layer, making the samples symmetric in the X and Y planes. The plate was a 50 mm x 50 mm x 3 mm slab of CF20 material. For these samples, the electric field vector is parallel to the layers of the sample during measurement. Figure 4 shows a rendering of these samples.

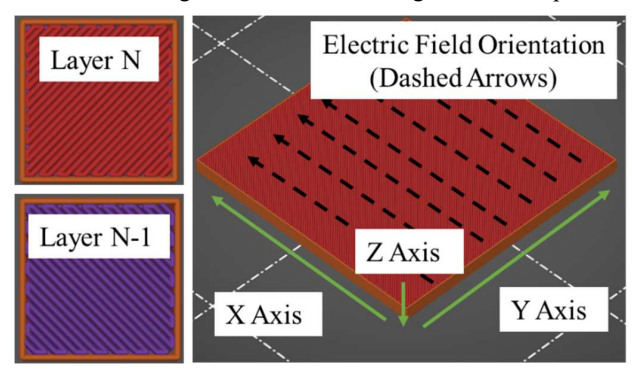


Fig. 4. (Left) Infill pattern used to print the slab sample. (Right) Orthographic view of the 3D printed slab sample with axes and electric field annotations.

B. Permittivity Measurements

Initially, the permittivity of the CF20 material was measured using the airline and OEWG methods. For this, the toroidal and slab samples were printed as discussed in Section III part A and then measured as outlined in Section II. The airline method resulted in a real permittivity between 5.3 and 5.8 for frequencies from 800 MHz to 18 GHz. The OEWG method resulted in a much higher permittivity between 22 and 30 for frequencies from 8.2 to 12.4 GHz. These results are shown in Figures 5 and 6.

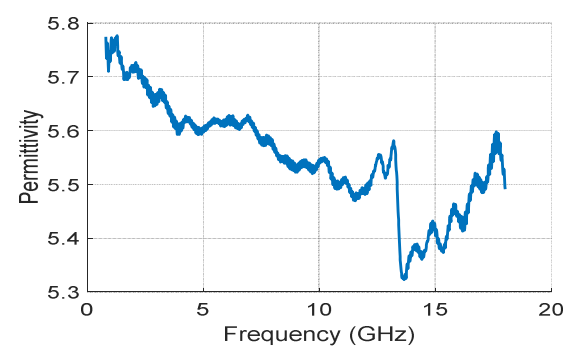


Fig. 5. The airline method permittivity measurement results.

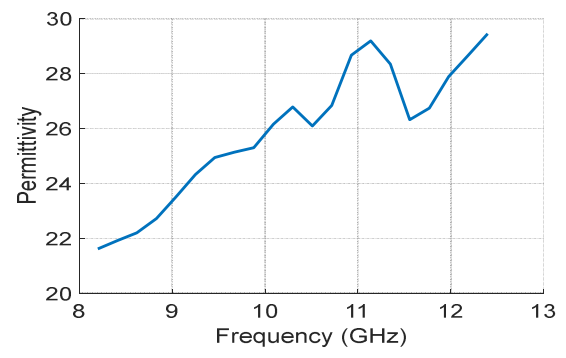


Fig. 6. The OEWG method permittivity measurement results.

During these initial permittivity measurements, the printed samples were assumed to be isotropic and as such, it was expected that each measurement method, airline, and OEWG, should yield similar permittivities for the printed CF20 material. As shown, Figures 5 and 6 disagree with each other and exhibit strong dispersion. This dispersion is most likely nonphysical and is attributed to errors in the initial measurement (see the results of the capacitive measurement below giving practically frequency-independent permittivity). As such this initial measurement only provides a rough estimate of the CF20's permittivity. Despite this, the disagreement between measurement methods suggested that this initial isotropic assumption may be incorrect and that the CF20 material may be anisotropic when printed as described in section III part A.

To investigate this anisotropy, 3 cubic samples were printed as discussed above. After printing, copper foil was then attached to opposite faces of the cubic samples to create a parallel plate capacitor that has an electric field vector parallel to a major axis of each sample. Figure 7 shows these copper-foiled samples. In Figure 7, the solid green line represents the layers of the sample, and the arrows represent the electric field during measurement. In this case and as illustrated in Figure 7, the electric field is parallel to the layers of the sample for the X and Y orientations but is perpendicular to the layers of the sample for the Z orientation.

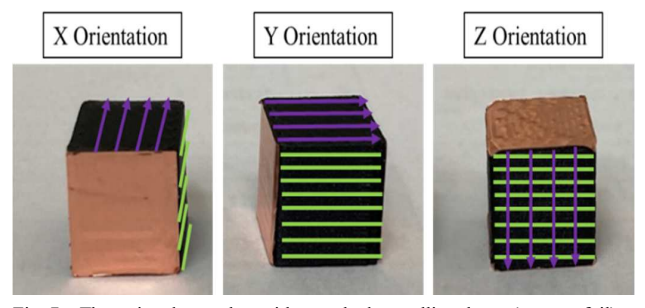
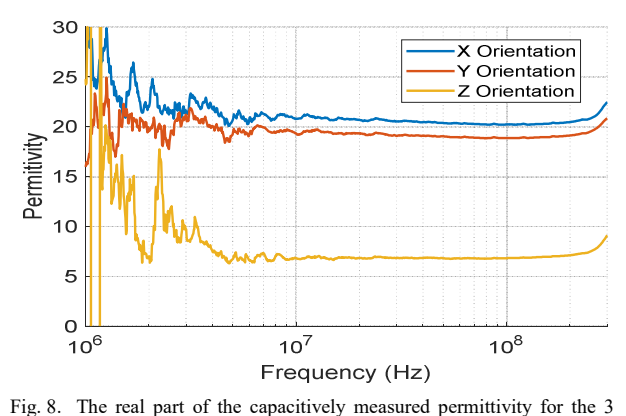


Fig. 7. The printed samples with attached metallic plates (copper foil) creating a parallel plate capacitor aligned with the respective major axis of the sample. The solid green line represents the layers of the sample, and the purple arrows represent the electric field during measurement.

After these samples were constructed, the permittivity of each sample was measured for each orientation, X, Y, and Z. Figures 8 and 9 show the real part of the permittivity and the loss tangent for each of these measurements. As shown in Figures 8 and 9, the real part of the permittivity and the loss tangent components are almost frequency independent for frequencies from 10-200 MHz.



rig. 8. The real part of the capacitively measured permittivity for the scubic samples from 1-300 MHz.

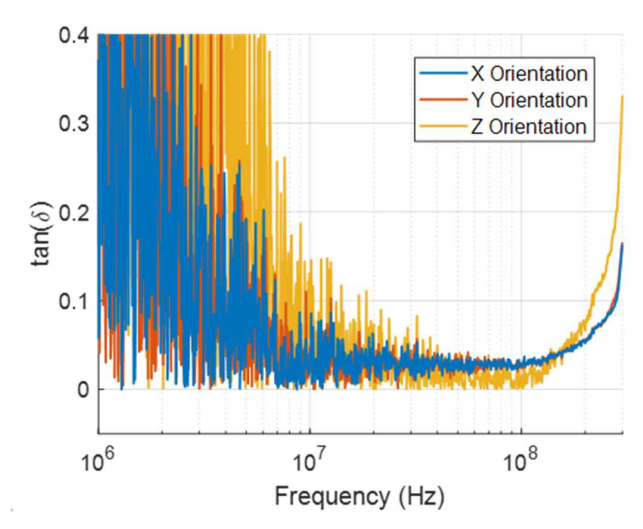


Fig. 9. The loss tangent for the 3 cubic samples from 1 - 300 MHz.

Below 10 MHz, reliable results could not be achieved due to dynamic range limitations inherent to the VNA when measuring the high impedance of the sample. Above 200 MHz, the increase of the permittivity is attributed to the structural resonance of the sample (due to the parasitic inductance) which makes (3) invalid.

Despite these limitations, the measurement results clearly indicate a very large difference in the permittivity components and disagree with the data previously reported in [10]. A possible reason for this disagreement is that most likely in [10], the direction of the electric field in the capacitance measurement was across the layers, such as in the Z orientation in Figure 7, and thus a low value of the permittivity was measured.

Moreover, because the cubic samples are symmetric with respect to the X and Y orientations, it is expected that the X and Y orientation measurements yield similar results. As shown in Figure 8, a reasonable agreement is observed between these results thereby matching the expectation. Further, the X and Y orientation measurements also agree with the initial OEWG measurements and disagree with the airline measurements. The converse of this is true for the Z orientation measurement. The reason for this is due to the anisotropy of the CF20 material when printed as discussed above. When the electric field is oriented perpendicular to the printed layers of a sample, as is the case for the Z orientation of the cubic sample and airline measurements (formally in the airline the electric field is oriented parallel to the layers, but since it is perpendicular to the parallel vertical walls, effectively it is the orientation similar to Z for the cubic samples), a low permittivity is measured. When the electric field is oriented parallel to the printed layers of a sample, like in the X and Y orientations of the cubic samples and the OEWG measurement, a high permittivity is measured.

To be clear, this difference in the measured permittivity components for the cubic samples is not induced by the electric field orientation. Rather, it is inherent to the CF20 material when printed in a manner such as that discussed in this work. The different electric field orientations merely allow one to measure the permittivity components of this material and observer this anisotropy from the measurements.

IV. APPLICATION TO DIELECTRIC RESONATOR

Understanding the material properties of a dielectric is critically important if the material is to be properly used for high-frequency devices. This is especially true for an anisotropic material like the CF20 presented in this work, where a lack of awareness of the anisotropy may lead to a drastically different performance than intended. To demonstrate this point, a simple dielectric-filled cavity resonator was considered. Specifically, the resonator is a 10 x 10 x 10 mm cubic cavity filled with CF20 dielectric material (Figure 10). The resonator is excited by a 3.7 mm pin which is partially embedded within the cavity. Unfortunately, the capacitive permittivity measurement method cannot be used at frequencies above several hundreds of MHz due to the inherent structural resonances of the samples. Because of this. the values of the permittivity matrix elements at the higher frequencies are not directly available. Therefore, a hypothesis that the permittivity components at high frequencies (up to 20 GHz) are similar to the values obtained by the capacitive method was tested by comparing the result of measurements to simulations.

To achieve this, three simulation cases with varying dielectric fill permittivities were considered:

- 1. Low permittivity isotropic dielectric fill ($\varepsilon_r = 6.5$).
- 2. High permittivity isotropic dielectric fill ($\varepsilon_r = 22$).
- 3. Anisotropic dielectric fill ($\varepsilon_{xr} = 23$, $\varepsilon_{yr} = 22$, $\varepsilon_{zr} = 6.8$)

For case 3 above, the values of the permittivity components were tuned slightly relative to the low-frequency values to ensure a better match of the first resonance between the simulated and measured reflection coefficients.

This resonator was created by 3D printing the dielectric fill in the same manner as the cubic samples described above, and then covering the faces of the printed dielectric fill with copper tape to create the conductive shell of the resonator. An SMA connector was used to excite the resonator. Figure 10 shows the CST model of the resonator and the fabricated resonator used for measurement. Reflection coefficient measurements (S_{11}) were performed using a calibrated N5225A PNA.

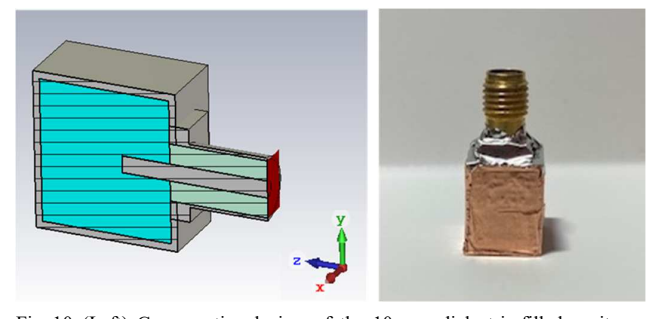


Fig. 10. (Left) Cross-sectional view of the 10 mm dielectric-filled cavity resonator simulation model. (Right) The fabricated dielectric-filled cavity resonator.

Figures 11 – 13 show a comparison of the simulated reflection coefficients for the low permittivity isotropic fill, high permittivity isotropic fill, and anisotropic fill cases, respectively to the measured reflection coefficient of the dielectric-filled cavity resonator.

In Section III, the CF20 material is clearly shown to be anisotropic. As such, in Figures 10-12, it is expected that the measurement and simulation will only show good agreement

for the simulation conducted assuming anisotropy (Figure 12), and not those that assume isotropic properties (Figures 10 and 11). It is clear that there is good agreement between the measured reflection coefficient of the cavity and the anisotropic dielectric fill simulation (Figure 12), and not with the isotropic simulations (Figures 10 and 11). This further supports the conclusions that:

- The CF20 material, when printed in the manner described by this work, is anisotropic.
- The high frequency permittivity of the CF20 material is similar to the low frequency permittivity determined by the capacitive method and is supported by the results obtained via the OEWG method.

Moreover, these results emphasize the importance of fully understanding the material properties of the dielectrics used for a high-frequency microwave device design.

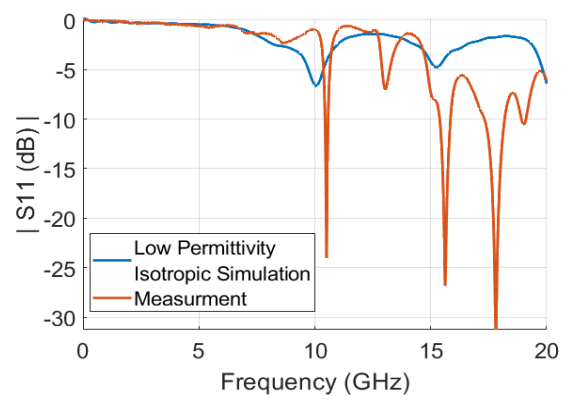


Fig. 11. Comparison of the low permittivity ($\varepsilon_r=6.5$) isotropic dielectric fill simulation to the measurement

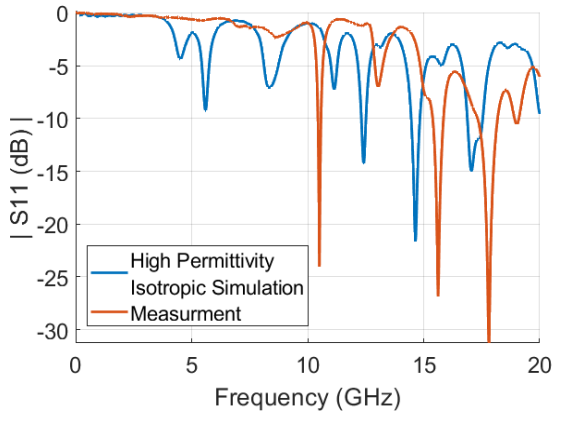


Fig. 12. Comparison of the high permittivity ($\varepsilon_r = 22$) isotropic dielectric fill simulation to the measurement

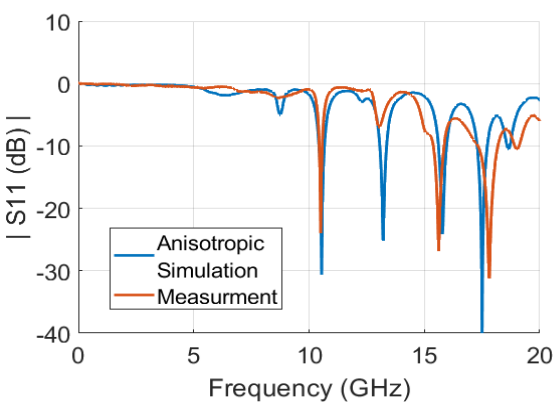


Fig. 13. Comparison of the anisotropic dielectric fill simulation to the measurement

V. CONCLUSION

In this paper, the measured diagonal elements of the permittivity matrix for 3D printed XT-CF20 dielectric samples are reported. It is well known that 3D printed objects are mechanically anisotropic and as such, may also exhibit similar behavior electromagnetically. However, many works assume that the 3D printed materials are electromagnetically isotropic. As shown in this work, this assumption is not always true as the CF20 material used in this work is clearly anisotropic and has surprisingly high permittivity components. The reason for this anisotropy is related to the infill structure of the printed sample. Due to this, permittivity measurements of CF20 samples constructed with different sample geometries or infill patterns may produce drastically different results.

Future work on this topic will include further study of the effect of infill pattern on the anisotropy of a printed sample, measurement of the permittivity components for higher frequencies, and consideration of other carbon fiber-loaded filaments.

ACKNOWLEDGMENTS

This work is supported in part by the National Science Foundation under Grant No. IIP-1916535.

REFERENCES

- [1] R. Mi et al., "3D Printed Electromagnetic Absorber Built with Conductive Carbon-filled Filament," 2021 IEEE International Joint EMC/SI/PI and EMC Europe Symposium, 2021, pp. 266-271, doi: 10.1109/EMC/SI/PI/EMCEurope52599.2021.9559309.
- [2] K. G. Kjelgård, D. T. Wisland and T. S. Lande, "3D Printed Wideband Microwave Absorbers using Composite Graphite/PLA Filament," 2018 48th European Microwave Conference (EuMC), 2018, pp. 859-862, doi: 10.23919/EuMC.2018.8541699.
- [3] M. Kamkar, M. Amini, S. Ghaderi, A. Ghafarkhah, A. A. Hosseini and M. Arjmand, "Advanced 3D Printed Conductive Polymer Nanocomposites for Electromagnetic Shielding," 2021 IEEE Sensors, 2021, pp. 1-4, doi: 10.1109/SENSORS47087.2021.9639856.
- [4] R. Kronberger and V. Wienstroer, "3D-printed FSS using printing filaments with enclosed metal particles," 2017 Progress in

- Electromagnetics Research Symposium Fall (PIERS FALL), 2017, pp. 808-811, doi: 10.1109/PIERS-FALL.2017.8293245.
- [5] R. Kronberger and P. Soboll, "New 3D printed microwave metamaterial absorbers with conductive printing materials," 2016 46th European Microwave Conference (EuMC), 2016, pp. 596-599, doi: 10.1109/EuMC.2016.7824413.
- [6] M. Mirzaee, S. Noghanian, L. Wiest and I. Chang, "Developing flexible 3D printed antenna using conductive ABS materials," 2015 IEEE International Symposium on Antennas and Propagation & USNC/URSI National Radio Science Meeting, 2015, pp. 1308-1309, doi: 10.1109/APS.2015.7305043.
- [7] Z. Khan, H. He, X. Chen and J. Virkki, "Dipole Antennas 3D-printed from Conductive Thermoplastic Filament," 2020 IEEE 8th Electronics System-Integration Technology Conference (ESTC), 2020, pp. 1-4, doi: 10.1109/ESTC48849.2020.9229736.
- [8] K. Alsirhani, K. A. Abdalmalak, C. S. Lee, G. Santamaría-Botello, D. Segovia-Vargas and L. E. García-Muñoz, "Dielectric Resonator Antenna Fed by Tapered Dielectric Rod Waveguide for 5G mm-Wave Applications," 2020 IEEE International Symposium on Antennas and Propagation and North American Radio Science Meeting, 2020, pp. 149-150, doi: 10.1109/IEEECONF35879.2020.9329488.
- [9] A. Eid, B. Tehrani, J. Hester, H. Xuanke and M. M. Tentzeris, "Nanotechnology-Enabled Additively-Manufactured RF and Millimeter-wave Electronics," 2018 IEEE 13th Nanotechnology Materials and Devices Conference (NMDC), 2018, pp. 1-4, doi: 10.1109/NMDC.2018.8605849.
- [10] D. Kalaš, K. Šíma, P. Kadlec, R. Polanský, R. Soukup, J. Řeboun, and A. Hamáček, "FFF 3D Printing in Electronic Applications: Dielectric and Thermal Properties of Selected Polymers," *Polymers*, vol. 13, no. 21, p. 3702, Oct. 2021.

- [11] colorFabb, "colorFabb XT-CF20", Technical datasheet, Aug. 2017.
 [Online]. Available:
 https://colorfabb.com/media/datasheets/tds/colorfabb/TDS_E_ColorFabb_XT_CF20.pdf [Accessed Nov. 29, 2021]
- [12] Standard test methods for AC loss characteristics and permittivity (dielectric constant) of solid electrical insulation. West Conshohocken, PA: ASTM International, 2018.
- [13] A. M. Nicolson and G. F. Ross, "Measurement of the Intrinsic Properties of Materials by Time-Domain Techniques," in *IEEE Transactions on Instrumentation and Measurement*, vol. 19, no. 4, pp. 377-382, Nov. 1970, doi: 10.1109/TIM.1970.4313932.
- [14] W. B. Weir, "Automatic measurement of complex dielectric constant and permeability at microwave frequencies," in *Proceedings of the IEEE*, vol. 62, no. 1, pp. 33-36, Jan. 1974, doi: 10.1109/PROC.1974.9382.
- [15] M. T. Ghasr, D. Simms and R. Zoughi, "Multimodal Solution for a Waveguide Radiating Into Multilayered Structures—Dielectric Property and Thickness Evaluation," in *IEEE Transactions on Instrumentation and Measurement*, vol. 58, no. 5, pp. 1505-1513, May 2009, doi: 10.1109/TIM.2008.2009133.
- [16] M. Kempin, M. T. Ghasr, J. T. Case and R. Zoughi, "Modified Waveguide Flange for Evaluation of Stratified Composites," in *IEEE Transactions on Instrumentation and Measurement*, vol. 63, no. 6, pp. 1524-1534, June 2014, doi: 10.1109/TIM.2013.2291952.
- [17] Keysight, 85071B Materials Measurement Software User's Manual (Apr93), 1993 (8)
- [18] J. Vasquez, Jubilee Project wiki. [Online]. Available: https://jubilee3d.com/index.php?title=Main_Page. [Accessed: 07-Jan-2022].